22nd International Congress of Mechanical Engineering (COBEM 2013)
November 3-7, 2013, Ribeirão Preto, SP, Brazil

FEM (Finite Element Method) Simulation of the Three-Dimensional Boundary Layer Close to a Rotating Semi-spherical Electrode in Electrochemical Cells

Rachel Manhães de Lucena
Norberto Mangiavacchi
Group of Environmental Studies for Water Reservatories – GESAR/State University of Rio de Janeiro, Rua Fonseca Teles, 121, 20940-200, Rio de Janeiro, RJ, Brazil
rachel.lucena@gmail.com, norberto.mangiavacchi@gmail.com

Gustavo R. Anjos
Massachusetts Institute of Technology, 77 Massachusetts Avenue Room NW12-306 MA 02139-4301, Cambridge, USA
gustavo.rabello@gmail.com

José Pontes
Metallurgy and Materials Engineering Department – Federal University of Rio de Janeiro, PO Box 68505, 21941-972 Rio de Janeiro, RJ, Brazil
jopontes@metalmat.ufrj.br

Abstract. *In this work we consider the steady boundary layer close to semi-spherical electrodes, developed by constant viscosity 1* $\mathbf{M}$ $\mathbf{H_2SO_4}$ *electrolytes in electrochemical cells. The principles of a semi-analytical solution consisting of a power series of the polar angle, multiplying functions describing the dependency of the velocity componentes on the radial coordinate are first discussed. A numerical Finite Element Method (FEM) procedure is then proposed to obtain the velocity profiles of the boundary layer, for polar angles* θ *(southern direction) ranging* $0 \leq \theta \leq \pi/2$*. Spatial discretization of the diffusive and pressure terms is performed by the Galerkin method, and of the material derivative, through the Semi-lagrangian method. The numerical code, developed in C++, uncouples the velocity and pressure through the discrete projection method. Conjugate gradient method is used to solve the velocity whereas pressure is solved with the generalized minimal residual method (GMRES). The results obtained are compared with the semi-analytical solution obtained by the power series method.*

Keywords: *corrosion, rotating disk flow, semi-spherical electrode, finite element method, boundary layer*

1. INTRODUCTION

The hydrodynamic field developed close to the axis of a large rotating disk belongs to the restricted class of problems admitting a analytical or semi-analytical similarity solution of the hydrodynamic equations (von Kármán, 1921). The angular velocity imposed to the fluid at the surface gives rise to a centrifugal effect and to a radial flow outwards. Continuity requires that the flow is replaced by an incoming one that approaches the disk. Close to the surface, the axial velocity of the incoming flow is reduced and the centrifugal effect appears. Among the applications of von Kármán's rotating disk flow we mention aerodynamics, flow in turbomachineries, crystal growth, heat transfer in electronic equipments, surgical devices circulatory assistance.

von Kármán's flow find an important application in applied electrochemistry, where cells using iron rotating disk electrodes are widely used due to the fact of requiring an easily built experimental setup and to the existence of von Kármán's solution. Based on this solution the current in the cell is theoretically evaluated and compared to the experimental results. A caveat of such experimental apparatus results from the fact that, particularly at high current regimes, dissolution of the iron electrode in the 1 $\mathbf{M}$ $\mathbf{H_2SO_4}$ solution of the electrolyte endamages the geometry of the electrode surface and the electrode no longer can be used. An alternative to overcome the problem consists in using rotating semi-spherical electrodes, which keep the geometry in the dissolution process. However, no similarity solution exists for the complete hydrodynamic equations exits for this case. First, a boundary layer approximation is required for the equations governing the flow in the neighborhood of the electrode and second, a solution is found, in terms of a power series of the polar angle, multiplying functions describing the dependency of the velocity componentes on the radial coordinate.

Setups with both rotating disk and rotating semi-spherical electrodes have been used by the group of Applied Electrochemistry of the Federal University of Rio de Janeiro (PEMM/COPPE/UFRJ). The experimental setup features cylindrical beaker containing the electrolyte, a counter-electrode consisting of a platinum mesh disposed along the cell sidewalls, a reference electrode and rotating disk or semi-spherical working electrode. The working electrode consists of a $5mm$ diameter iron electrode laterally lined with a resin, resulting in a cylindrical rod with $10mm$ diameter. The current flow through the $5mm$ diameter lower surface of the rod. A rotating semi-spherical electrode cell is schematically shown

in Fig. 1.

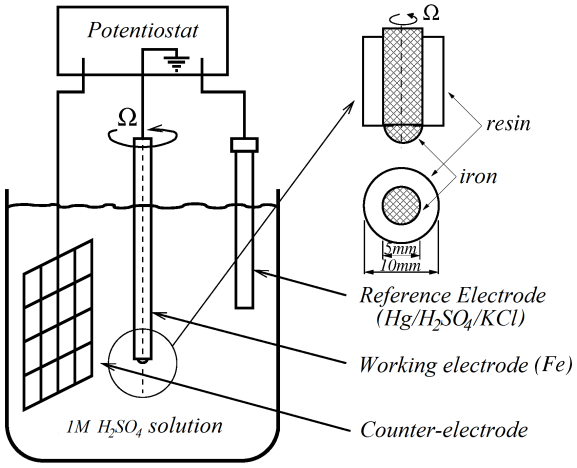

Figure 1. Electrochemical cell with a rotating semi-spherical electrode

The flow close to a rotating semi-sphere, or rotating semi-sphere electrode was studied by Lamb (1932), Bickley (1938), Howarth (1951), Godinez (1996) and Barcia *et al.* (1998). Godinez (1996) addressed the steady flow close to a rotating semi-spherical electrode by obtaining a solution in the form of an expansion for the velocity components, in terms of a power series of the polar angle. This solution satisfies the boundary layer equations for the flow close to a rotating semi-sphere. The steady boundary layer equations were also solved by a finite differences scheme.

In this work we briefly review the principles of the power series solution for the steady solution of the boundary layer developed by constant viscosity electrolytes close to rotating semi-spherical electrodes and propose a numerical Finite Element (FEM) procedure to obtain the velocity profiles for polar angles θ (southern direction) ranging $0 \leq \theta \leq \pi/2$. The results are compared to the ones obtained by Godinez, as a step towards validating the code. We used as a method to solve the finite element method (FEM) and validate the results by comparison with Godinez's results.

2. METHODOLOGY

2.1 Power Series Method

This method consists in finding solution in terms of a power series of the variables describing the system state and obeying an equation or a system of differential equations.

Equations governing Godinez (1996) the flow close to a rotating sphere are the continuity and momentum equations of the velocity components along the radial and polar directions (r, θ, ϕ).

The hydrodynamic boundary layer equations, applicable to the flow close to a rotating semi-sphere obtained under the assumption of high Reynolds numbers are given by:

$$\frac{\partial v_r}{\partial r} + \frac{1}{r_0}\frac{\partial v_\theta}{\partial \theta} + \frac{\cot\theta}{r_0} v_\theta = 0 \tag{1}$$

$$v_r \frac{\partial v_\theta}{\partial r} + \frac{v_\theta}{r_0}\frac{\partial v_\theta}{\partial \theta} - \frac{\cot\theta}{r_0} v_\phi^2 = \nu \frac{\partial^2 v_\theta}{\partial r^2} \tag{2}$$

$$v_r \frac{\partial v_\phi}{\partial r} + \frac{v_\theta}{r_0}\frac{\partial v_\phi}{\partial \theta} + \frac{\cot\theta}{r_0} v_\theta v_\phi = \nu \frac{\partial^2 v_\phi}{\partial r^2}. \tag{3}$$

In the above equations, r_0 is the radius of the semi-sphere and ν, the kinematic viscosity of the fluid. Boundary conditions for Eqs. (1)-(3) are, in $r = r_0$: $v_r = v_\theta = 0$ and $v_\phi = r_0\bar{\Omega}\sin\theta$, where $\bar{\Omega}$ is the steady angular velocity imposed to the electrode.

Upon assuming symmetry along the azimuthal direction ϕ, we express the velocity components in terms of the polar angle and the nondimensional radial coordinate η given by:

$$v_\theta = r_0\bar{\Omega}F(\theta,\eta), \quad v_\phi = r_0\bar{\Omega}G(\theta,\eta), \quad v_r = (\nu_\infty\bar{\Omega})^{1/2}H(\theta,\eta) \quad \text{and} \quad \eta = \left(\bar{\Omega}/\nu\right)^{1/2}(r - r_0). \tag{4}$$

The nondimensional equivalent equations in directions η and θ, respectively, radial and meridional directions of a semi-spherical, are:

$$\frac{\partial H}{\partial \eta} + \frac{\partial F}{\partial \theta} + \cot\theta F = 0 \tag{5}$$

$$H\frac{\partial F}{\partial \eta} + F\frac{\partial F}{\partial \theta} - \cot\theta G^2 = \nu\frac{\partial^2 F}{\partial \eta^2} = 0 \quad (6)$$

$$H\frac{\partial G}{\partial \eta} + F\frac{\partial G}{\partial \theta} + \cot\theta FG = \nu\frac{\partial^2 G}{\partial \eta^2} = 0. \quad (7)$$

The power series method was applied to the system of Eqs. (5)-(7) where the nondimensional functions are given by:

$$F(\theta,\eta) = \sum_{i=1}^{n}\theta^{2i-1}F_{2i-1}(\eta), \quad G(\theta,\eta) = \sum_{i=1}^{n}\theta^{2i-1}G_{2i-1}(\eta), \quad H(\theta,\eta) = \sum_{i=1}^{n}\theta^{2i-2}H_{2i-1}(\eta) \quad \text{and}$$

$$\cot\theta = \frac{1}{\theta} - \frac{\theta}{3} - \frac{\theta^3}{45} - \frac{2\theta^5}{945} - \cdots.$$

We restrict the number of terms of the series expansion of functions F, G, H and $\cot\theta$ to $n = 10$, obtaining thus ten systems of differential equations, numerically solved by Newton's method.

2.2 Finite Element Method

The Finite Element method is a numerical technique of approximations (and discretizations). It is a important tool to solve problems that involve partial differential equations. The domain of problem is subdivided in sub-domains named finite elements, and over this elements are applied functions of interpolation that approximate to solution this sub-domain, the set of sub-domain's solutions is the approximate solution of the problem.

2.2.1 Governing Equations and Variational Formulation

The equations that model the incompressible flow of a newtonian fluid with constant viscosity and determine the hydrodynamic field nondimensional form are given by:

$$\frac{D\mathbf{v}}{Dt} = -\frac{1}{\rho}\nabla p + \frac{1}{Re}\nabla\cdot\left[\nu\left(\nabla\mathbf{v} + \nabla\mathbf{v}^T\right)\right] \quad \text{and} \quad (8)$$

$$\nabla\cdot\mathbf{v} = 0, \quad (9)$$

where $\mathbf{v}(\mathbf{x},\mathbf{t})$ is velocity vector, $p(\mathbf{x},t)$ is the pressure, ρ is the specific mass of the fluid, ν is the kinematic viscosity of the fluid and Re is the Reynolds number. Equation (8) is the Navier-Stokes equation and Eq. (9) is the continuity equation.

Boundary conditions to the Eqs (8) and (9) are $\mathbf{v} = \mathbf{v}_\Gamma$ on Γ_1, $\mathbf{v}_t = 0$ and $\sigma^{nn} = 0$ on Γ_2, respectively to velocity and pressure.

The variational formulation is obtained by properly weighting the Navier-Stokes equations and continuity equation. We obtain:

$$\int_\Omega \frac{D\mathbf{v}}{Dt}\cdot\mathbf{w}\,d\Omega - \frac{1}{\rho}\int_\Omega p\left[\nabla\cdot\mathbf{w}\right]\,d\Omega + \frac{1}{Re}\int_\Omega\left[\left(\nabla\mathbf{v} + \nabla\mathbf{v}^T\right)\right] : \nabla\mathbf{w}^T\,d\Omega = 0 \quad (10)$$

$$\int_\Omega \left[\nabla\cdot\mathbf{v}\right] q\,d\Omega = 0. \quad (11)$$

where functions $\mathbf{w}$ and q are *weighting functions* defined in the space $\mathcal{V} := \left\{\mathbf{w}\in\mathcal{H}^1(\Omega) \mid \mathbf{w} = 0 \text{ in } \Gamma_c\right\}$, where $\mathbf{u_c}$ is the essential boundary condition value, Γ_c a possible boundary for the domain Ω, $\mathcal{H}^1(\Omega) := \left\{\mathbf{u}\in\mathcal{L}^2(\Omega)\middle|\frac{\partial\mathbf{u}}{\partial x_i}\in\mathcal{L}^2(\Omega), i = 1,\ldots,n\right\}$ and $\mathcal{L}^2(\Omega)$ is the *Lebesgue space*, i. e., the space of all *square integrable* functions.

2.2.2 Semi-discrete Galerkin method

The semi-discrete Galerkin Method provides a partial discretization where the functions that approximate a solution for the governing equations (Eqs.(10) and (11)) comprise a linear combination of shape functions depending on the time of functions intended to depend on the space coordinates. Following this procedure we denote by NV and NP the number of velocity, pressure and concentration nodes, respectively, of the discrete grid of elements of the original domain Ω. The following semi-discrete approximation functions are obtained:

$$v_x(\mathbf{x},t) \approx \sum_{i=1}^{NV}u_i(t)N_i(\mathbf{x}), \quad v_y(\mathbf{x},t) \approx \sum_{i=1}^{NV}v_i(t)N_i(\mathbf{x}), \quad v_z(\mathbf{x},t) \approx \sum_{i=1}^{NV}w_i(t)N_i(\mathbf{x}) \quad \text{and}$$

$$p(\mathbf{x},t) \approx \sum_{i=1}^{NP}p_i(t)P_i(\mathbf{x}),$$

where the coefficients u_i, v_i, w_i and p_i denote continuous functions in the time (t) and functions $N_i(\mathbf{x})$ and $P_i(\mathbf{x})$ are interpolation functions at specified positions $\mathbf{x}$ for the velocity and pressure, respectively.

The discretized system becomes, in matrix form:

$$\begin{aligned} \mathbf{M}\dot{\mathbf{v}} + \frac{1}{Re}\mathbf{K}\mathbf{v} - \mathbf{G}\mathbf{p} &= 0 \\ \mathbf{D}\mathbf{v} &= 0, \end{aligned}$$

where

$$\mathbf{M} = \begin{bmatrix} \mathbf{M_x} & 0 & 0 \\ 0 & \mathbf{M_y} & 0 \\ 0 & 0 & \mathbf{M_z} \end{bmatrix}, \quad \mathbf{K} = \begin{bmatrix} \mathbf{K_X} & \mathbf{K_{xy}} & \mathbf{K_{xz}} \\ \mathbf{K_{yx}} & \mathbf{K_Y} & \mathbf{K_{yz}} \\ \mathbf{K_{zx}} & \mathbf{K_{zy}} & \mathbf{K_Z} \end{bmatrix}, \quad \mathbf{G} = \begin{bmatrix} \mathbf{G_x} & \mathbf{G_y} & \mathbf{G_z} \end{bmatrix}^T,$$

$$\mathbf{K_X} = 2\mathbf{K_{xx}} + \mathbf{K_{yy}} + \mathbf{K_{zz}}, \quad \mathbf{K_Y} = \mathbf{K_{xx}} + 2\mathbf{K_{yy}} + \mathbf{K_{zz}}, \quad \mathbf{K_Z} = \mathbf{K_{xx}} + \mathbf{K_{yy}} + 2\mathbf{K_{zz}},$$

$$\mathbf{D} = \begin{bmatrix} \mathbf{D_x} & \mathbf{D_y} & \mathbf{D_z} \end{bmatrix}, \qquad \dot{\mathbf{v}} = \begin{bmatrix} \dot{\mathbf{u}} & \dot{\mathbf{v}} & \dot{\mathbf{w}} \end{bmatrix}^T \qquad \text{and} \quad \mathbf{v} = \begin{bmatrix} \mathbf{u} & \mathbf{v} & \mathbf{w} \end{bmatrix}^T.$$

2.2.3 Semi-lagrangian method

The semi-lagrangian method has been widely used since the $80`s$ in the solution of convective problems. The main favorable features are stability and the large time steps allowed.

One can observe the use of a discrete representation of the substantial derivative in the discretized weak form of the governing equations. In this section we apply the semi-lagrangian method to the substantial derivatives of the governing equations. We obtain:

$$\frac{D\mathbf{v}}{Dt} = \frac{\mathbf{v}_i^{n+1} - \mathbf{v}_d^n}{\Delta t} \tag{12}$$

The global matrix system takes the following discrete form:

$$\mathbf{M}\left(\frac{\mathbf{v}_i^{n+1} - \mathbf{v}_d^n}{\Delta t}\right) + \frac{1}{Re}\mathbf{K}\mathbf{v}^{n+1} - \mathbf{G}p^{n+1} = 0 \tag{13}$$

$$\mathbf{D}\mathbf{v}^{n+1} = 0, \tag{14}$$

where $\mathbf{v}_d^n = \mathbf{v}^n(x_d, t^n)$ and x_d refers to the starting point in the time $t^n \leq t \leq t^{n+1}$ with initial condition $x(t^{n+1}) = x_i$.

2.2.4 Elements of the mesh

The element implemented to calculate the components velocity (from Navier-Stokes equations) was the MINI tetrahedral element, this element has one plus degree of freedom located in the centroid of the tetrahedron. We used a third degree interpolation polynomial because the finite element is a tetrahedron.

2.2.5 Discrete projection method

The discrete projection method based in the LU decomposition is obtained from block decomposition of resulting linear system. Velocity and pressure are decoupled after discretization in the position and in the time of the governing equations.

Equations (13) and (14) form a equations system that can be represented by:

$$\begin{bmatrix} B & -\Delta t G \\ D & 0 \end{bmatrix} \cdot \begin{bmatrix} \mathbf{v}^{n+1} \\ p^{n+1} \end{bmatrix} = \begin{bmatrix} r^n \\ 0 \end{bmatrix} + \begin{bmatrix} bc_1 \\ bc_2 \end{bmatrix} \tag{15}$$

where $\mathbf{v}^{n+1} = [u_1^{n+1}, \ldots, u_{Nu}^{n+1}, v_1^{n+1}, \ldots, v_{Nv}^{n+1}, w_1^{n+1}, \ldots, w_{Nw}^{n+1}]^T$, $p^{n+1} = [p_1^{n+1}, \ldots, p_{Np}^{n+1}]^T$, Nu, Nv, Nw and Np are the unknown numbers for velocity in the directions x, y and z and pressure, respectively.

The matrix B is given by:

$$B = M + \frac{\Delta t}{Re}K, \tag{16}$$

the vector r^n is given by:

$$r^n = -\Delta t(M\mathbf{v}_d^n) + M\mathbf{v}^n \tag{17}$$

and bc_1 and bc_2 are the boundary conditions.

Using the canonical LU factorization by blocks on the system (15), we obtain:

$$\begin{bmatrix} B & 0 \\ D & \Delta t D B^{-1} G \end{bmatrix} \cdot \begin{bmatrix} I & -\Delta t B^{-1} G \\ 0 & I \end{bmatrix} \cdot \begin{bmatrix} \mathbf{v}^{n+1} \\ p^{n+1} \end{bmatrix} = \begin{bmatrix} r^n \\ 0 \end{bmatrix} + \begin{bmatrix} bc_1 \\ bc_2 \end{bmatrix} \tag{18}$$

As we have B^{-1}, the system (18) gives rise to the *Uzawa* method (Chang *et al.*, 2002) which uses exact factorization. But its solution is very expensive computing cost due the fact the inversion of B for each iteration. Alternatively we use the approximate factorization which approximates the matrix B^{-1} for B_L^{-1}, where B_L is the *lumped* matrix. The *lumping* technique consists in attributions sum of a line and locate it in the main diagonal.

3. RESULTS

In this section we presented the results of this work. We consider the domain of the semi-sphere as $R = r_0 + dr$, where r_0 is the physical radius of the semi-sphere and dr is the thickness of the mesh. We used the follows dimensions: $R = 55$, i.e., $r_0 = 40$ and $dr = 15$.

3.1 Computational mesh for a rotating semi-spherical electrode

The computational mesh used in the FEM's simulations is shown in the Fig. 2, this mesh mimics the geometry semi-spherical of the electrode for the three-dimensional numerical simulations.

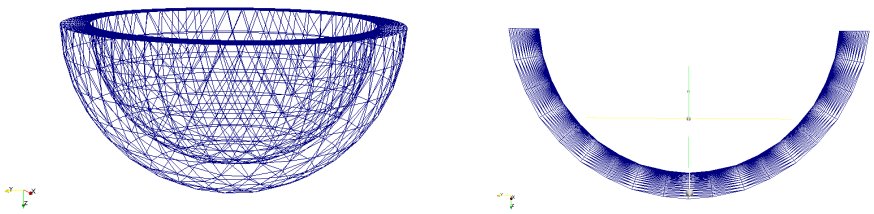

(a) Representation of computational mesh (b) Sectioned mesh

Figure 2. Computational mesh

3.2 Boundary conditions

Figure 3 help us comprehension as the boundary conditions were applied. In the solid surface (side A of Fig. 3) were applied boundary conditions: $v_z = 0$, $v_x = -\bar{\Omega} y$ and $v_y = \bar{\Omega} x$. In the side B we applied Neumann's boundary condition at velocity ($\mathbf{n} \cdot \nabla \mathbf{v} = 0$) and Dirichlet's boundary condition for the pressure ($p = 0$). And the sides C and D were applied the pressure equal to zero.

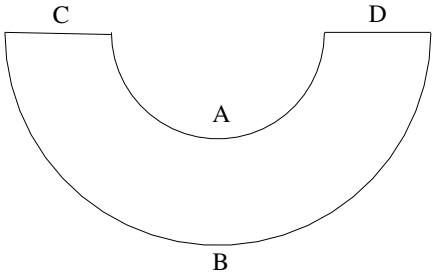

Figure 3. Representation of boundary conditions of semi-spherical electrode

3.3 Qualitative results

In this section we present the behavior of the fluid, we show the flow close to a rotating semi-spherical electrode. Figures 4, 5 and 6 show that the velocity field are correct and for angles (θ) superior to $60°$, the solution presents one recirculation because we have applied pressure equal to zero at equator.

We can also observe to the development of the boundary layer from the pole of the semi-sphere to the equator.

Velocity magnitude

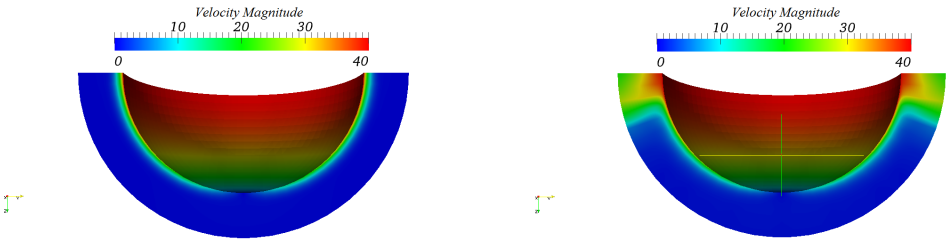

(a) $t = 0$ (b) $t = 15.0$

Figure 4. Velocity magnitude at two times

The z component of the velocity

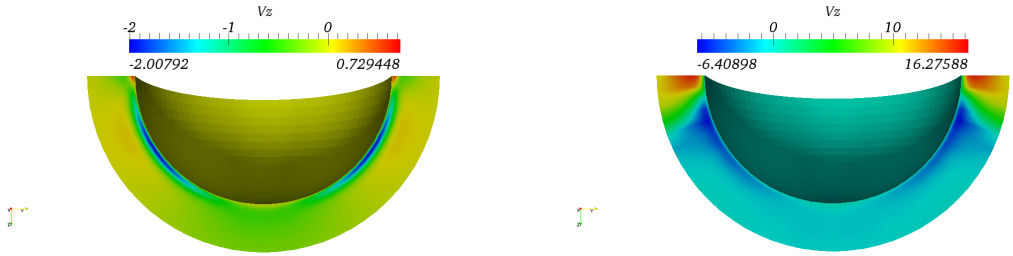

(a) $t = 0$ (b) $t = 15.0$

Figure 5. z component of the velocity at two times

The x component of the velocity

The behavior of the flow in the directions x and y are symmetric, thus we show only in the direction x.

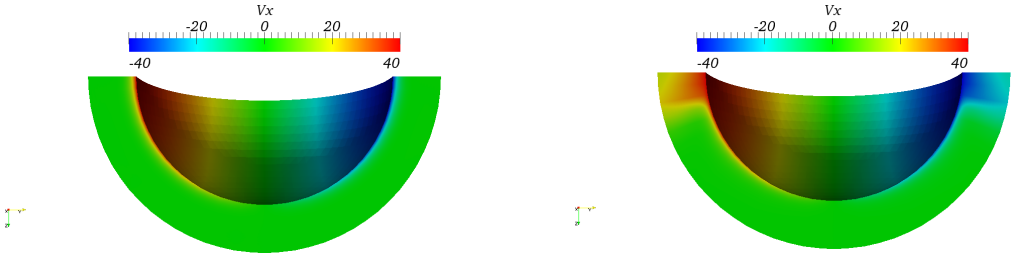

(a) $t = 0$ (b) $t = 15.0$

Figure 6. x component of the velocity at two times

3.4 Quantitative results

Figure 7 shows the numerical results obtained by FEM's simulations compared with the semi-analytical results obtained by Godinez (1996). We present the velocity profiles for angles $\theta = 20°$, $\theta = 40°$, $\theta = 60°$ and $\theta = 80°$.

The Fig. 7 confirms that has been stated in Sec. 3.3 when we said that the qualitative results are consistent with the behavior of flow close to a rotating semi-sphere.

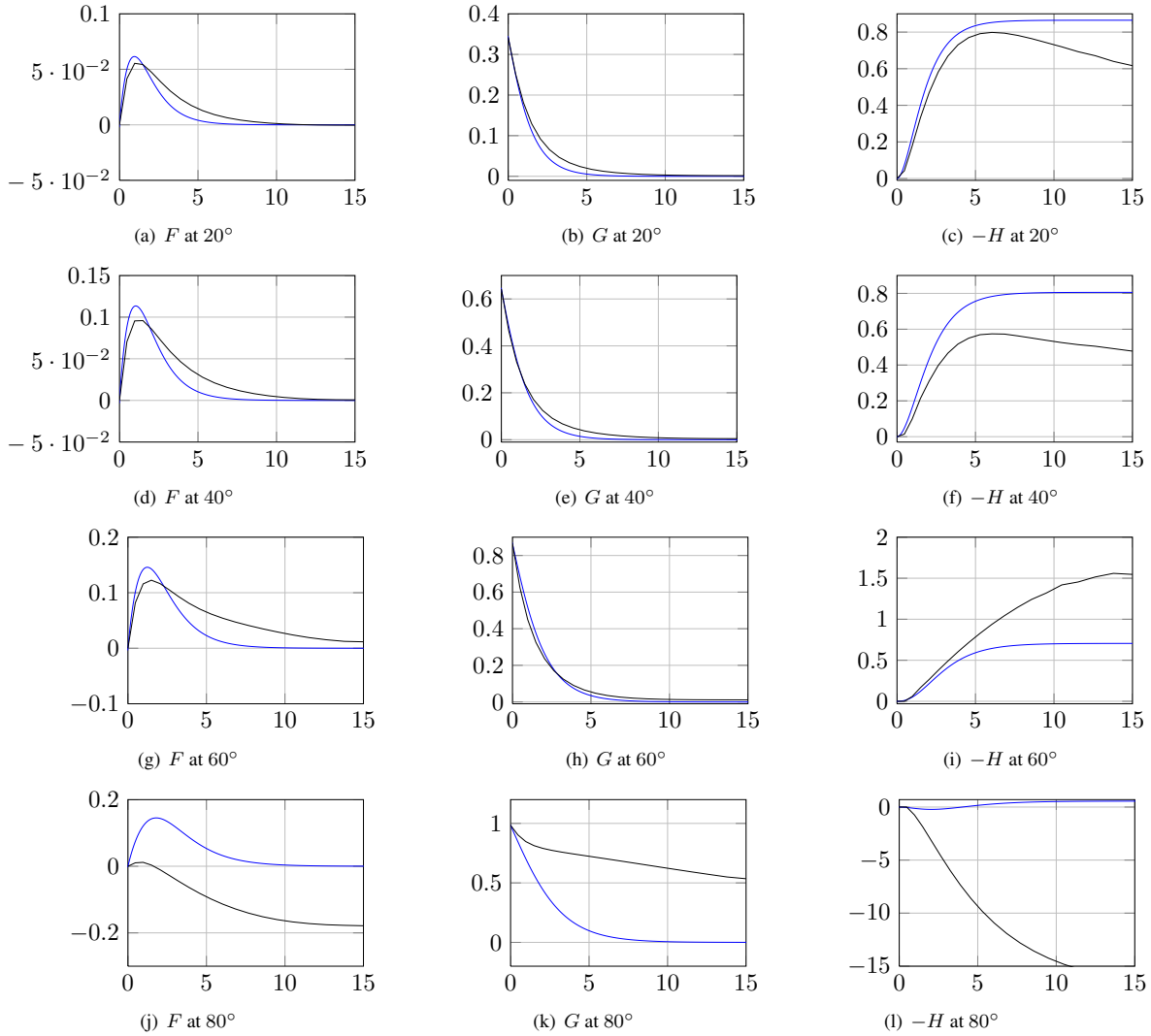

Figure 7. Semi-analytical and numerical solution comparing for the profiles F, G and $-H$ at 20°, 40°, 60° and 80°. Legend: — Semi-analytical solution and — Numerical solution.

Tables 1 to 4 show for semi-analytical and numerical solutions the maximal value for F profile, initial point for G profile and the minimal value for H profile for different angles θ.

Table 1. Values for $\theta = 20°$

Profiles	Semi-analytical solution	Numerical solution
F	0.0615	0.0554
G	0.3420	0.3420
H	-0.8649	-0.8979

Table 2. Values for $\theta = 40°$

Profiles	Semi-analytical solution	Numerical solution
F	0.1134	0.0958
G	0.6428	0.6428
H	-0.8058	-0.5741

Table 3. Values for $\theta = 60°$

Profiles	Semi-analytical solution	Numerical solution
F	0.1458	0.1226
G	0.8660	0.8660
H	-0.7058	-1.5592

Table 4. Values for $\theta = 80°$

Profiles	Semi-analytical solution	Numerical solution
F	0.1451	0.0117
G	0.9848	0.9848
H	-0.5580	-0.0060

Tables 1 to 4 show the discrepancy confirmation observed by graphical analyzing of semi-analytical and numerical solutions showed in Fig. 7.

Figure 8 shows absolute error obtained between semi-analytical and numerical solutions of F, G and H profiles for the angles $\theta = 20°, 40°, 60°$ and $80°$. As previously mentioned, we can to verify with accuracy and to state the numerical solution distance obtained by semi-analytical solution required, which the errors are 10^{-1} to 10^{1} order.

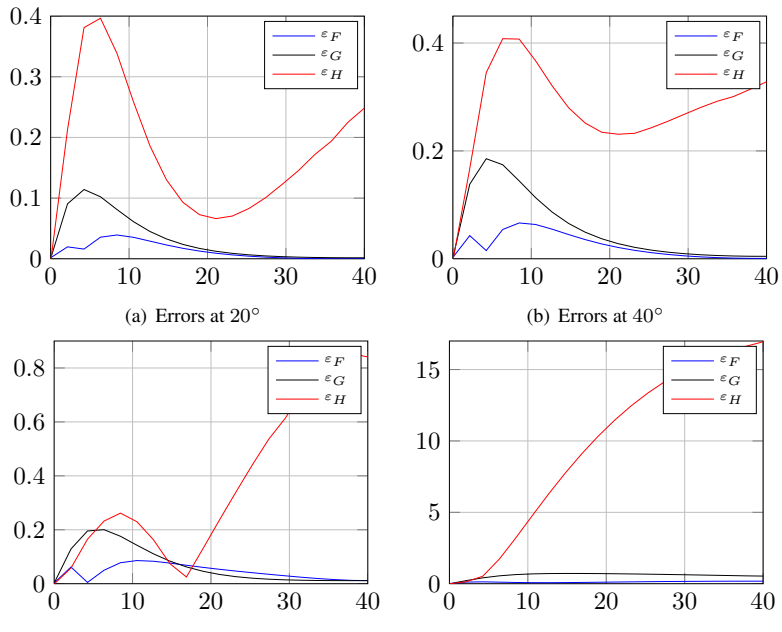

(a) Errors at 20° (b) Errors at 40°

(c) Errors at 60° (d) Errors at 80°

Figure 8. Errors for the profiles F, G and H at $20°$, $40°$, $60°$ and $80°$

The results obtained for the functions F and G to $60°$ are good, where the function F from a certain radius becomes negative in order to equilibrate the mass balance. And the results for the function H tend towards an asymptotic value as expected from the semi-analytical solution.

For angles greater than $60°$ the results are not good because it is the region where has a recirculation of the flow.

4. CONCLUSIONS

The results presented are good but they are not sufficient, we need to simulate more cases increasing the radius of the rotating semi-spherical because this determine the Reynolds number involved in the problem. As we want to simulate the flow close the boundary layer we should increase the Reynolds number as a result of the domain of the problem but it requires greater computing cost.

5. ACKNOWLEDGEMENTS

The authors acknowledge financial support from the Brazilian agency CAPES. They also acknowledge the Group of Environmental Studies for Water Reservatories – GESAR/State University of Rio de Janeiro, where most simulations here presented were performed.

6. REFERENCES

Anjos, G.R., 2007. *Solução do Campo Hidrodinâmico em Células Eletroquímicas pelo Método dos Elementos Finitos*. Dissertação de M.Sc., COPPE/UFRJ, Rio de Janeiro, RJ, Brasil.

Barcia, O., Godinez, J. and Lamego, L., 1998. "Rotating hemispherical electrode: Accurate expressions for the limiting current and the convective warbug impedance". *Journal of The Electrochemical Society*, Vol. 145, No. 12, pp. 4189–4195.

Batchelor, G.K., 2000. *An Introduction to Fluid Dynamics*. Cambridge University Press, Cambridge, 1st edition.

Bickley, W.G., 1938. *Phil. Mag.*, Vol. 7, No. 25, p. 746.

Chang, W., Giraldo, F. and Perot, B., 2002. "Analysis of an exact fractional step method". *Journal of Computational Physics*, , No. 179, pp. 1–17.

Godinez, J.G.S., 1996. *Eletrodo semi-esférico rotatório: teoria para o estado estacionário*. Tese de D.Sc., COPPE/UFRJ, Rio de Janeiro, RJ, Brasil.

Howarth, L., 1951. *Phil. Mag.*, Vol. 7, No. 42, p. 1308.

Hughes, T.J.R., 1987. *The Finite Element Method: Linear Static and Dynamic Finite Element Analysis*. Prentice-Hall, New Jersey, 1st edition.

Lamb, H., 1932. *Hydrodynamics*. Cambridge University Press, Cambridge.

Oliveira, G.C.P., 2011. *Estabilidade Hidrodinâmica em Células Eletroquímicas pelo Método de Elementos Finitos*. Dissertação de M.Sc., COPPE/UFRJ, Rio de Janeiro, RJ, Brasil.

von Kármán, T., 1921. "Uber laminare und turbulente reibung". *ZAMM*, Vol. 1, No. 4, pp. 233–252.

7. RESPONSIBILITY NOTICE

The authors are the only responsible for the printed material included in this paper.